Materials Science and Engineering C 73 (2017) 198–205

Contents lists available at ScienceDirect

Materials Science and Engineering C

journal homepage: www.elsevier.com/locate/msec

Immobilization of heparin/poly-L-lysine microspheres on medical grade high nitrogen nickel-free austenitic stainless steel surface to improve the biocompatibility and suppress thrombosis

Menghua Li [b,1], Haide Wu [a,b,1], Yi Wang [b], Tieying Yin [b], Hans Gregersen [b], Xiaojuan Zhang [b], Xiaoling Liao [a], Guixue Wang [a,*]

[a] Chongqing Key Laboratory of Nano/Micro Composite Materials and Devices, School of Metallury and Materials Engineering, Chongqing University of Science and Technology, Chongqing, China
[b] Key Laboratory of Biorheological Science and Technology, Ministry of Education, State and Local Joint Engineering Laboratory for Vascular Implants, Bioengineering College, Chongqing University, Chongqing, China

ARTICLE INFO

Article history:
Received 10 September 2016
Received in revised form 21 November 2016
Accepted 11 December 2016
Available online 15 December 2016

Keywords:
High nitrogen nickel-free austenitic stainless steel
Heparin
Microsphere
Blood compatibility
Coronary stent

ABSTRACT

Thrombosis formation, restenosis, and delayed endothelium regeneration continue to be a challenge for coronary artery stent therapy. To improve the hemocompatibility of cardiovascular implants and to selectively direct vascular cell behavior, a novel heparin/poly-L-lysine microsphere was developed and immobilized on a dopamine-coated surface. We chose medical grade high nitrogen nickel-free austenitic stainless steel as the stent material since it has better biocompatibility. The stability and structural characteristics of the microspheres changed with the heparin: poly-L-lysine concentration ratio. Antithrombin III binding was significantly enhanced. Furthermore, for plasma coagulation tests, the activated partial thromboplastin time and thrombin time were prolonged and depended on the heparinfunction. The modified exhibited excellent stability and anticoagulant activity, and efficiently accelerated endothelialization and anticoagulation. This work has potential application for the design of coronary artery stent surfaces tailored for vascular cell behavior.

1. Introduction

For the cardiovascular system, coronary heart disease is the largest threat and the main reason of death and impairment of health [1–2]. The treatment of coronary heart disease includes three categories: drug therapy, surgical treatment and interventional treatment. Percutaneous coronary intervention is an important treatment for coronary heart disease due to small trauma, less pain, and achievement of rapid revascularization due to acute coronary syndrome in case of emergency [3–5]. At present, about 95% of patients have interventional therapy with stents [6]. Stent placement has become the main technology of interventional therapy. SUS316L, Co-Cr and platinum-chromium (Pr-Cr) are the most widely used coronary stent materials [7]. SUS316L and nitinol alloy may release nickel ions, which potentially can be toxic, leading to anaphylactic reaction and cancer [8–9]. Furthermore, SUS316L and nitinol alloy may cause thrombosis due to incompatibility with blood [10–11]. Li et al. [12] examined the biocompatibility of medical grade high nitrogen nickel-free austenitic stainless steel in vitro. The analysis of the mechanical properties and biocompatibility showed that medical grade high nitrogen nickel-free austenitic stainless steel might be used as alternative materials of stent.

Heparin (Hep) is the most commonly used anticoagulant drug and has also been widely used as an anticoagulant coating of material surfaces in contact with blood [13]. The anticoagunt properties of Hep depends on its specific interaction with antithrombin III (AT III), which causes a rapid inactivation of thrombin and other proteases involved in blood clotting [14]. Numerous studies have also shown that Hep can inhibit migration and proliferation of blood vessel cells, especially smooth muscle cells (SMCs) [15]. These in vitro data were further verified in animal testing and in clinical trials, demonstrating that a Hep-coated stent surface helps to prevent thrombosis and intimal hyperplasia [16]. In addition, early in the 1960s, Hep was shown to exhibit excellent performance as an anti-inflammatory drug in various inflammatory disease models [17]. The multifunctional properties of Hep are generally attributed to its interactions with various proteins. To date >100 Hep-binding proteins have been identified [18]. In different experimental setups, Hep may exhibit different or even opposite actions in directing cell behavior. For example, stromal cell-derived factor-1 a (SDF-1 a)-immobilized Hep coating promoted the recruitment of endothelial progenitor cells and SMCs, though the antiproliferante effect of Hep is apparently blocked after binding with the cytokine [19]. Moreover, Hep is considered to harm endothelial cells (ECs) [20]. However, our recent studies suggested that an appropriate Hep dosage selectively enhances

* Corresponding author.
E-mail address: wanggx@cqu.edu.cn (G. Wang).
[1] These authors contributed equally to this work.

http://dx.doi.org/10.1016/j.msec.2016.12.070
0928-4931/

ECs but inhibits SMC proliferation [21–22]. Hence, a heparinized surface with adequate drug density and release kinetics will inhibit thrombosis and restenosis but will not harm the endothelium. Sakiyama-Elbert [23] provided a relatively comprehensive overview of the incorporation of Hep into biomaterials. The most commonly used methods to conjugate Hep seem to be covalent immobilization or electrostatic binding [24]. The former is considered to be stable, but protein binding and anticoagulant activities are reduced due to the use of bioactive carboxylic groups for the immobilization chemistry and the reduced steric accessibility of the immobilized molecule [25]. Electrostatic binding does not harm Hep bioactivity, though burst release remains a major limitation due to the insufficient binding force. In addition, it still appears difficult to control the Hep binding density on the surface.

In this study, the Hep density gradient was constructed on a polydopamine-coated material surface with high stability and bioactivity. It was probed with respect to the behavior of platelets, plasma proteins, as well as ECs. Polydopamine is a mussel-inspired adhesive coating, which has become attractive in the biomaterials field due to its ability to form strong adhesive interactions with materials [26] and with functional biomolecules that contain amine groups [27]. However, Hep is a highly sulfated glycosaminoglycan, rich in hydroxyl, carboxyl and sulfo groups but almost free of amine groups, and hence does not directly bind to a dopamine-coated surface. In this study, a novel Hep immobilizing approach is introduced by covalently binding Hep/poly-L-lysine (PLL) microspheres onto dopamine-coated surface. A similar method has been adopted by Park et al. [28], though the protocol of microsphere preparation and the experimental system they used were very different from our work. As a cationic polymer of amino acids, PLL is commonly used for loading of negatively charged biomolecules, e.g. as gene vectors. Nevertheless, PLL shows a low level of transfection efficiency due to the tight interactions between PLL/DNA complexes [29]. The drawback of PLL in gene transfer could constitute an advantage in terms of immobilizing biomolecules on surfaces. In the present study, amine-rich PLL is mixed with negatively charged Hep to construct Hep/PLL microspheres. Microspheres with different Hep: PLL concentration ratios are subsequently immobilized onto polydopamine (PDA)-coated surfaces. The change in the exposed amine group on different microspheres directly influences the total amount immobilized and thereby creates a Hep density gradient surface. Taking the influence of exposed amine groups into consideration, we have demonstrated that the behavior of platelets and ECs can be selectively regulated over a certain Hep density range.

2. Materials and methods

2.1. HNS preparation

High nitrogen nickel-free stainless steel coupons (HNS, 15 mm diameter, provided by Chongqing Materials Research Institute Co. Ltd) were mirror-polished and ultrasonically cleaned twice with deionized water, acetone and absolute alcohol before use for 5 min each time.

2.2. Hep/PLL microsphere preparation and immobilization

The formation of Hep/PLL microspheres in phosphate buffered saline (PBS) is mainly driven by the electrostatic interaction between negatively charged Hep and positively charged PLL. In general, the particle system is considered moderately stable when the absolute value of the zeta potential is higher than 30 mV. The particle dispersion index (PDI) is another important indicator to evaluate the size distribution of the particles, and a smaller PDI indicated a better uniformity. Preparation of 5 mg ml^{-1}Hep solution and 0.5 mg ml^{-1}PLL solution was done with PBS as solvent under ultrasonic conditions for 5 min to create the suspension of Hep/PLL microspheres. For preparation of PDA coating, the HNS samples were immersed into 2 mg ml^{-1} PDA solution (dissolved in 10 mM Tris buffer, pH 8.5) at 20 °C for 12 h. Then the samples were ultrasonically washed three times with distilled water for 5 min each time, dried in the oven, and marked as one layer. The above operation was repeated twice more, for a total of three PDA layers to be grafted on the sample surfaces. Subsequently, the PDA-coated HNS samples were immersed into prepared Hep/PLL microsphere solutions and incubated at 20 °C for 12 h during gentle shaking. Finally, it was washed three times with distilled water for 5 min and freeze dried to construct Hep/PLL microsphere-immobilized samples.

2.3. Microsphere size and zeta potential analysis

The mean size, PDI, and the zeta potential of the Hep/PLL microspheres dispersed in PBS medium were determined by dynamic light scattering using a Zetasizer Nano-ZS90 (Malvern Ltd., Malvern, UK). Each measurement was repeated three times.

2.4. Characterization of microspheres fixed on dopamine

2.4.1. X-ray photoelectron spectrometer

The surface chemical elemental composition of PDA-coated and Hep/PLL microsphere-immobilized samples was studied by X-ray photoelectron spectroscopy (XPS, Kratos Ltd., UK) on an AXIS His spectrometer with a monochromatic Al Kα X-ray source (1486.6 eV photons, 150 W). The pressure in the chamber was $< 2 \times 10^{-9}$ Torr. The binding energy scale was referenced by setting the C_{1s} peak at 284.6 eV.

2.4.2. Atom force microscopy

The changes in surface topography before and after Hep/PLL microsphere immobilization were characterized by atom force microscopy (AFM, Nanowizard II, JPK Instruments, Berlin, Germany) in contact mode. AFM was done at room temperature and the images were processed by CSPM Imager software.

2.4.3. Water contact angle

Changes in surface hydrophilicity may cause quantitative and qualitative variations of absorbed proteins, which directly influence the biocompatibility of the materials. The static water contact angle on the samples were measured using a DSA100 Mk 2goniometer (Kruss GmbH, Germany) at room temperature. A droplet of deionized water was added to dried sample surfaces. The contact angle was calculated by a circle segment function of the DSA 1.8 software. There were four parallel samples in each group. For each sample, measurements were taken at least at three different sites.

2.4.4. Measurement coating thickness using metaloscope

Focal plane measurements of metaloscope can quantitate the thickness of polylactic acid matrix coatings accurately. Mosaic the coated sample with denture acrylic plates and water, and a longitudinal section on the surface of the sample was polished with a grinding machine. An optical microscope (Metallurgical Microscopy, MM) was used to show the boundary between coating and substrate materials, coating and inlays. The metaloscope images were obtained by charge coupled device,

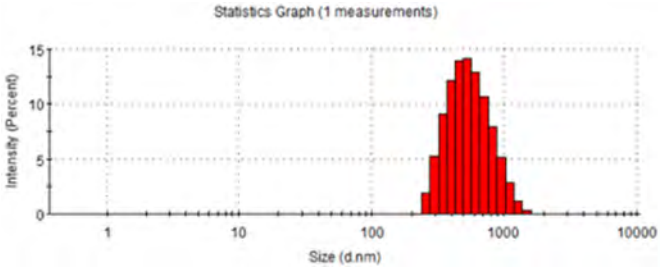

Fig. 1. The distribution of the microsphere size. The mean size of the Hep/PLL particles ranged from 300 nm to 1500 nm.

Table 1
Mean size and zeta potential of Hep/PLL microspheres.

	Size(nm)	Zeta potential(mV)	PDI
Microsphere	529	−39.4	0.083

the pictures were adjusted to standard size using Photoshop where brightness and contrast was adjusted to make the pictures clearer. For each picture, a 25 μm scale was marked at 400 times magnification. Four sites randomly distributed on the coat were selected. Drawing tools were used to mark the thicknesses as h1, h2, h3, and h4. The average thickness was computed.

2.5. Blood compatibility evaluation in vitro

2.5.1. Platelet adhesion

3.8% sodium citrate anticoagulant was added to fresh healthy rabbit blood at a ratio of 1:9. Platelet-rich plasma (PRP) was prepared by subjecting whole blood to centrifugation at 1200 rpm for 15 min. The samples were immersed in physiological saline, placed into the PRP, and incubated at 37 °C for 1 h. The samples were gently rinsed with PBS to remove non-adherent platelets and fixed in 2.5 vol.% glutaraldehyde solution at 4 °C for at least 1 h. This was followed by dehydration in ethanol/distilled water gradient mixture (20%, 50%, 70%, 90% and 100%) for 15 min in consecutive order. After freeze-drying for 24 h, the samples were coated with Au thin film. Scanning electron microscopy (SEM, Vega-LMH, Tescan, Czech) was used to observe the surface morphology of the samples. Five microscopic images were randomly selected, and total numbers of adhered platelets were counted.

2.5.2. Hemolysis rate test

The hemolysis rate test was carried out according to standard protocol (ISO 10993.4). The anticoagulant was added to the venous blood (10 ml). Blood and saline were mixed at a ratio of 4:5; 5 ml of extracts and 0.1 ml of diluted blood were added into each tube in a 37 °C water bath for 1 h. Then 5 ml of saline was added to 0.1 ml of blood as the negative control and 5 ml of distilled water was added to 0.1 ml of blood as the positive control. The solution in each tube was centrifuged at 3000 rpm for 5 min. The absorbance of the supernatant was examined and recorded by a UV–vis spectrophotometer (Du 800, Beckman Coulter) at a wavelength of 545 nm. The hemolysis rate was calculated as:

$$\mathrm{HR}(\%) = \frac{\mathrm{Dt}-\mathrm{Dnc}}{\mathrm{Dpc}-\mathrm{Dnc}} \times 100\%$$

where HR is the hemolysis rate, Dt the absorbance of samples, Dnc the absorbance of the negative control, and Dpc the absorbance of the positive control.

2.5.3. APTT, PT and TT

The activated partial thromboplastin time (APTT) and prothrombin time (PT) are generally considered as performance indicators measuring the efficacy of intrinsic and extrinsic coagulation pathways, respectively. The thrombin time (TT) is always used to determine the activity of fibrinolytic systems. APTT is highly sensitive to Hep due to the blocking effect of Hep on clotting factors Xa, XIa and IIa. Hep–AT III complex is generally considered as the most active inhibitor to clotting factor IIa and HNSIa, directly influencing the PT value. TT assay was done to evaluate the effect of microspheres on inhibition of thrombin-mediated fibrin formation. The APTT and TT were measured to evaluate the influence of sample surface on the coagulation system. 500 μl platelet poor plasma (PPP) was added to the samples and incubated at 37 °C for 30 min.

For the APTT test, 100 μl incubated PPP was transferred to the test tube. 100 μl APTT agent was added and it was incubated at 37 °C for 3 min. Subsequently 100 μl 0.025 M $CaCl_2$ was added and the clotting time was measured in an automatic blood coagulation analyzer (ACL-200, Beckman Coulter, USA).

For the PT and TT tests, 100 μl PT or TT reagent were added to the test tube. 100 μl incubated PPP was added and it was incubated at 37 °C for 3 min. Subsequently the clotting time was measured using an automatic blood coagulation analyzer.

2.6. Cellular compatibility evaluation in vitro

2.6.1. Cell culture and cellular morphological characterization

The human unbilical vascular endothelial cells (HUVECs) were cultured in PRMI1640 medium which contained 15% standard fetal bovine serum (FBS) at 5% CO_2 and 37 °C. HUVECs were seeded on the sample surfaces at an identical density of 5×10^4 cells ml^{-1} and incubated at 37 °Cat 5% CO_2 for 1 day. After washing with PBS solution three times, cells were fixed with 2.5% glutaraldehyde at 4 °C for at least 1 h. The treatment samples were dehydrated with 20, 50, 70, 90and 100% ethanol for 15 min in consecutive order. After freeze-drying for 24 h, the samples were coated with an Au thin film. SEM (Vega-LMH, Tescan, Czech Republic) was used to observe the cell morphology.

2.6.2. Cytotoxicity test

The relative growth rate (RGR) of HUVCs was evaluated by 3-(4,5-dimethyl-2-thiazolyl)-2,5-diphenyl-2-H-tetrazolium bromide(MTT, purchased from ICN, USA.) assay for assessment of cell proliferation. MTT assay involves a reduction reaction which reduces MTT reagent to formazan when incubated with viable cells. Thus, the absorbance of formazan indirectly reflected the level of cell metabolism. The stainless steel surface in contact with the cells produced corrosion products in the cell culture medium which affected the MTT test and increased the measurement error. Therefore, we selected the indirect contact method to assess cell proliferation [30–31]. The extract water was made from RPMI1640 medium containing 15% serum. The surface

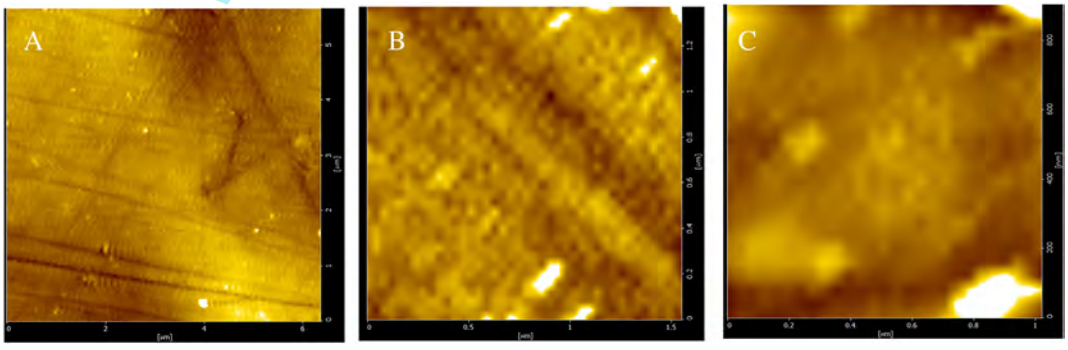

Fig. 2. AFM images of sample surface(A: HNS, B: HNS-PDA, C: HNS-PDA-Hep/PLL microsphere). Compared to the control group(A), the HNS-PDA(B) and HNS-PDA-Hep/PLL microsphere(C) surfaces showed varying degrees of bulging.

area ratio of the sample and the extraction medium was 1.25 ml cm^{-2} at 37 °Cat 5% CO_2 for at least 3 days before it was stored at 4 °C for later use. The cell suspension was seeded in 96-well plates at a concentration of 2–3 × 10^4cells/100 μl and cultured for 24 h until the cells were adherent. After incubating the cells in a humidified atmosphere with 5% CO_2 at 37 °C for 1, 3 and 5 days, respectively, 20 μl MTT solution (5 mg/ml) was added into each well. The plates were placed in an incubator at 37 °C for 4 h. 150 μl dimethylsulfoxide (DMSO, obtained from Sigma Chemical, USA.) was added after the supernatant medium was removed [32]. The plates were gently shaken for 10 min to make the crystals dissolve partially. The absorbance was examined and recorded by an enzyme micro-plate reader (Bio-tek ELHNS800, Vermont, USA) at a wavelength of 490 nm. The math model of RGR was computed as

$$RGR(\%) = \frac{As}{Ac} \times 100\%$$

where As is the absorbance of the treatments and Ac is the absorbance of the control.

2.7. NO release of HUVECs

HUVECs were seeded on the samples surface at a density of 4–5 × 100 cells ml^{-1}. All samples were transferred to 24-wells plates. Each well contained 500 μl cell suspension and was incubated at 37 °Cat 5% CO_2 for 1 day before the cell supernatant was obtained. Three duplicated treatments were done. The NO concentration assay was done by nitrate reductase. Processes and calculation methods and conversion formulas are in accordance with NO detection kit instructions [33].

$$NO(\mu mol/L) = \frac{OD_U - OD_B}{OD_S - OD_B} \times Cs \times N$$

where OD_U was the absorbance values of test tube, OD_S the absorbance value of the standard tube, ODB the absorbance value of blank tubes, C_S a standard concentration. NO standard concentration was 100 μmol/L. N was the dilution factor of the sample.

2.8. Total antioxidant capacity(T-AOC)

The grouping method was the same as NO release test. Processes and calculation methods and conversion formulas were in accordance with T-AOC kit.

$$T-AOC\left(mL^{-1}\right) = \frac{OD_U - OD_B}{0.01} \div 30 \times N \times n$$

where OD_U was the absorbance values of test tube, OD_C the absorbance value of control tube, N the dilution factor of the reaction system, and n the dilution factor of the origin sample.

2.9. Statistical analysis

The data obtained in this study are reported as means ± standard deviation. Data obtained from different treatment groups were statistically compared by statistical software SPSS 11.5 (SPSS, Inc., Chicago, Illinois). To reveal differences among the groups, one-way ANOVA followed by Tukey's test was done. Differences were considered significant if $P < 0.05$ and highly significant if $P < 0.01$.

Table 2
The surface topography after immobilization of different samples.

	HNS	HNS-PDA	HNS-PDA-Hep/PLL microspheres
Ra (nm)	6.31 ± 0.84	5.63 ± 0.24	8.10 ± 1.07
Rms (nm)	8.21 ± 0.67	8.07 ± 0.54	10.47 ± 0.97

Ra: arithmetic average of surface roughness (nm), Rms: mean square root of surface roughness (nm).

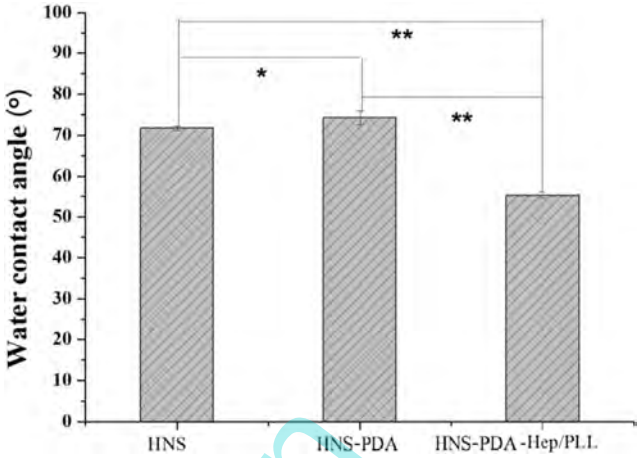

Fig. 3. Comparison of contact angle among HNS, HNS-PDA and HNS-PDA-Hep/PLL microsphere. The water contact angle of the pure material surface was 71.74 ± 0.58, which increased to 74.26 ± 1.74.55.24 ± 0.80after coating PDA and fixed microspheres, respectively. * and ** indicate significant difference ($P < 0.05$) and highly significant difference ($P < 0.01$).

3. Results

3.1. Size and zeta potential of microspheres

The mean size of the Hep/PLL particles ranged from 300 nm to <1500 nm (Fig. 1). The PDI value was 0.179 (Table 1), which showed acceptable uniformity of Hep/PLL microspheres.

3.2. Characterization of microspheres fixed on dopamine

3.2.1. AFM images of microsphere-immobilized surface

AFM is used to detect the surface topography after immobilization of different samples. A relatively uniform particle structure was observed on the immobilized surface which suggested that the microspheres

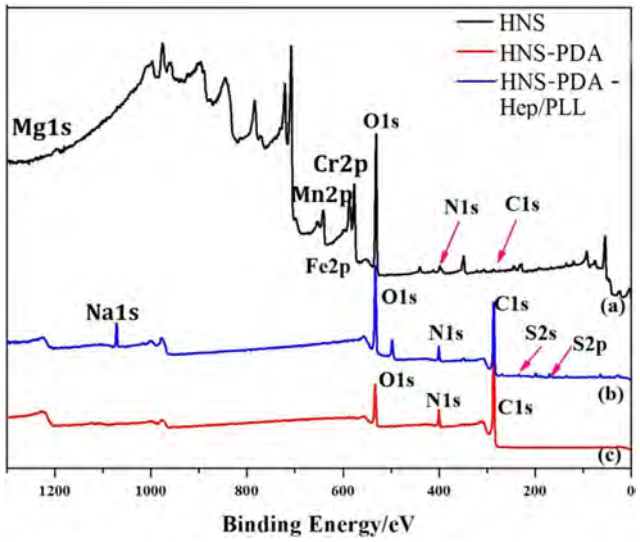

Fig. 4. The XPS spectra of samples HNS, HNS-PDA and HNS-PDA-Hep/PLL microsphere. The PDA was prepared with Tris buffer containing C, N element. The C and N elements in (b), (c) are nearly the same. Figure (a) and (c) shows that no Fe, Mn, Cr or other elements are detected in the PDA deposited sample. This indicates that the PDA deposited layer has a good compactness.

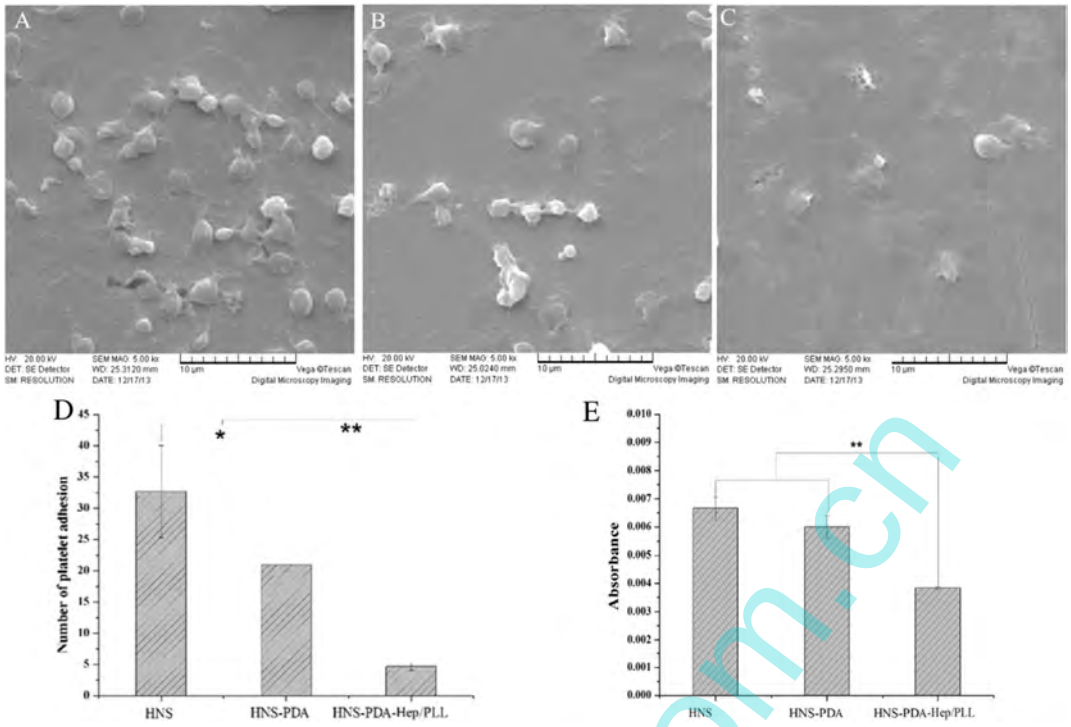

Fig. 5. Comparison of adherent platelet numbers and hemolytic rate of different samples. (A, B, C) Morphology of adherent platelets on the different surfaces(×5000 magnification), SEM images of surfaces show the microstructure, which large amounts of platelet aggregated on HNS and HNS-PDA sample surfaces (A and B), and the adherent platelets mainly exhibited spreading dendritic and fully spreading shape. In contrast, the number of platelets on immobilized microspheres was significantly decreased (C), and the adherent platelets displayed round shape and maintained the original shape. (D), Quantification of adherent platelet numbers, it is in agreement with the SEM results that platelets of HNS-PDA-Hep/PLL microsphere were significantly less than that of HNS-PDA and HNS surface. (E), Quantification of hemolysis rate of different samples, the hemolysis rate of HNS-PDA-Hep/PLL microsphere were highly significantly smaller than that of HNS-PDA and HNS. HNS and HNS-PDA surface can easily cause platelet adhesion and activation. * and ** indicate significant difference ($P < 0.05$) and highly significant difference ($P < 0.01$).

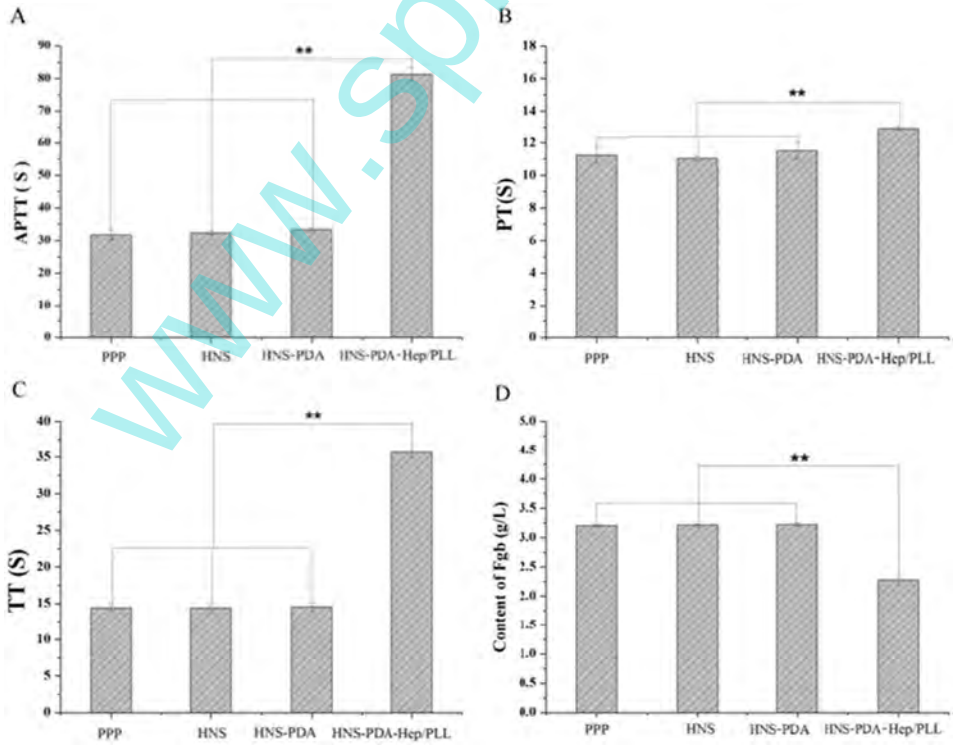

Fig. 6. APTT, PT, TT and Fbg of different samples surfaces. (A, B, C), The mean APTT, PT, TT value of HNS-PDA-Hep/PLL microspheres was prolonged by approximately 50 s, 2 s and 20 s in comparison with HNS and HNS-PDA. This indicated that Hep/PLL microsphere-immobilized surfaces exert a favorable effect on preventing fibrin-induced platelet adhesion and achieve a significant improvement in the anticoagulant property. (D), Quantification the surface fibrinogen (Fbg) content of each sample, the surface Fbg content of HNS and HNS-PDA was almost the same as that for PPP· HNS-PDA-Hep/PLL microsphere surface Fbg was significantly reduced. * and ** indicate significant difference ($P < 0.05$) and highly significant difference ($P < 0.01$).

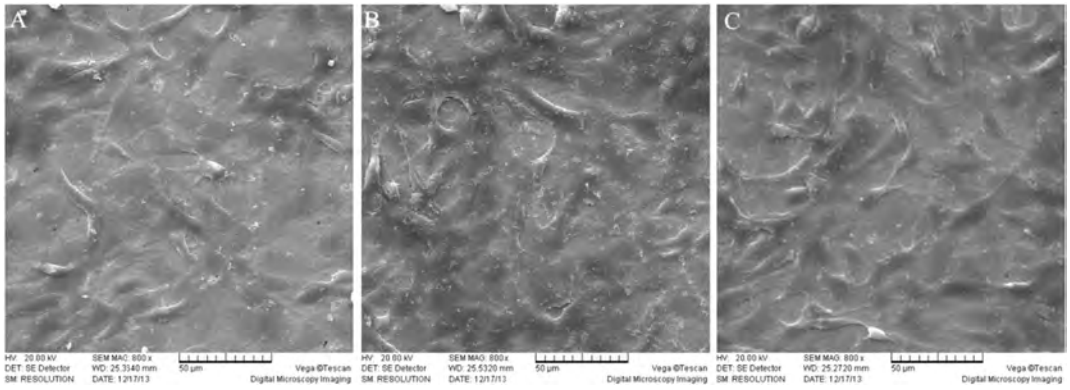

Fig. 7. The morphology of HUVECs after 1 day of culture on different samples incubated for 24 h at 37 °C. The HUVEC cells on the surface of different samples almost formed a single layer and kept their natural original shape, spindle or irregular triangular, extending freely, without significant difference among them.

possessed adequate stability. Nevertheless, micro-spraying enable the microspheres to maintain excellent conformation after immobilization. Fig. 2 is an AFM image showing microspheres immobilized on different sample surfaces obtained by tapping mode. Compared to the control group, the HNS-PDA and HNS-PDA-Hep/PLL microsphere surfaces showed varying degrees of bulging on the two-dimensional AFM images. The size of the fixed microspheres of the HNS-PDA-Hep/PLL group was larger than that of the HNS-PDA group (Table 2).

Compared to pure stainless steel, both the Ra and Rms values of HNS-PDA were decreased. However, after fixation of microspheres, the surface roughness increased a little.

3.2.2. Water contact angle

The water contact angle was measured to evaluate the surface hydrophilicity before and after microsphere immobilization. Fig. 3 shows the changes in water contact angle between nickel-free stainless steel surface coated PDA and fixed microspheres with PDA deposited. The water contact angle of the pure material surface was 71.74 ± 0.58, which increased to 74.26 ± 1.74 after coating PDA. This phenomenon may due to the highly hydrophobic benzene ring structure of PDA. The water contact angle of fixed microspheres was 55.24 ± 0.80. The heparin and PLL molecules containing large number of hydrophilic groups like -COOH, -NH_2 and -SO_3, decreased the water contact angle of the sample surface significantly compared to HNS and HNS-PDA. None of the three angles were >90°, demonstrating the hydrophilic nature.

3.2.3. XPS

The XPS wide-scan spectra of dopamine-coated, microsphere-immobilized and origin material surfaces are shown in Fig. 4. New S2s (234.6 eV), S2p (168.8 eV) and Na1s peaks appeared in the spectrum after microsphere immobilization. Thus, Hep/PLL microspheres were immobilized onto the PDA-coated surface. The content of O and S elements on the surface of microsphere samples were increased significantly. This is due to the heparin molecules rich in -COOH, -OH and -SO_2, containing quantity of O element and a small amount of S element.

3.3. Blood compatibility evaluation in vitro

3.3.1. Platelet adhesion

The amount and the activation profile of adherent platelets are considered key indicators for evaluating the hemocompatibility of the surface of a material. In general, platelet morphology was related to their activation level, with the typical shape of round, dendritic, spreading dendritic, spreading, and fully spreading that corresponded to the activation stage from minor to major. SEM images of platelet morphology showed that large amounts of platelet aggregated on HNS and HNS-PDA sample surfaces (Fig. 5A, B), and the adherent platelets mainly exhibited spreading dendritic and fully spreading shape. This indicated significant activation and poor hemocompatibility. In contrast, the number of platelets on immobilized microspheres was significantly decreased (Fig. 5C), and the adherent platelets displayed round shape and maintained the original shape. This indicated minor activation and excellent anticoagulant property. Five horizons of SEM images were randomly selected, and the numbers of platelet adhesion were statistical analyzed (Fig. 5D). In agreement with the SEM results, the surface platelets of the sample fixed with microspheres counted significantly lower than HNS and HNS-PDA surface platelets. Furthermore, platelets of HNS-PDA were significantly less than that of HNS surface. HNS and HNS-PDA surface can easily cause platelet adhesion and activation. The sample fixed with microspheres platelet indicated a significant inhabitation in adhesion and activation.

3.3.2. Hemolysis rate test

Data from the hemolysis rate test are shown in Fig. 5E. Surface hemolysis rate of HNS, HNS-PDA and HNS-PDA-Hep/PLL microspheres were all <5%. Hence they satisfied the reference standard for the National Biological Safety Evaluation of Hemolysis implant biomaterials. Hemolysis rate of samples fixed microspheres was smaller than HNS and HNS-PDA. It can be concluded that the coating layer possesses non-hemolytic effect and good blood compatibility.

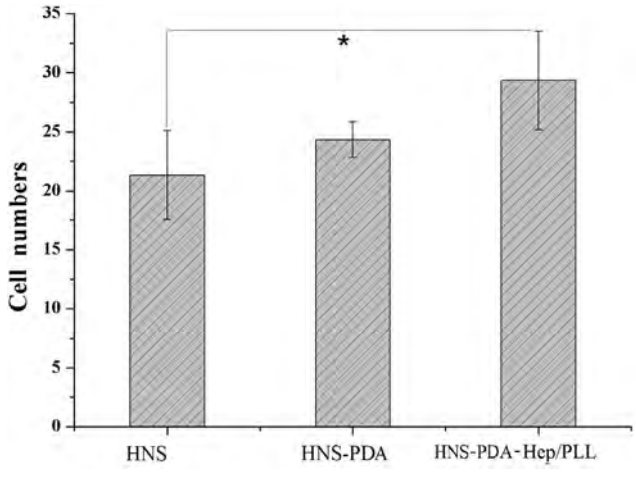

Fig. 8. Number of HUVECs adhered to the samples surfaces. Five SEM views (800× magnification) of each group were selected randomly to make statistical analysis for the adhesion of cells. Adhesion cell numbers were significantly different between HNS-PDA-Hep/PLL microspheres and HNS-PDA ($P < 0.01$), and with no significant difference between HNS-PDA and HNS($P > 0.05$). * and ** indicate significant difference ($P < 0.05$) and highly significant difference ($P < 0.01$).

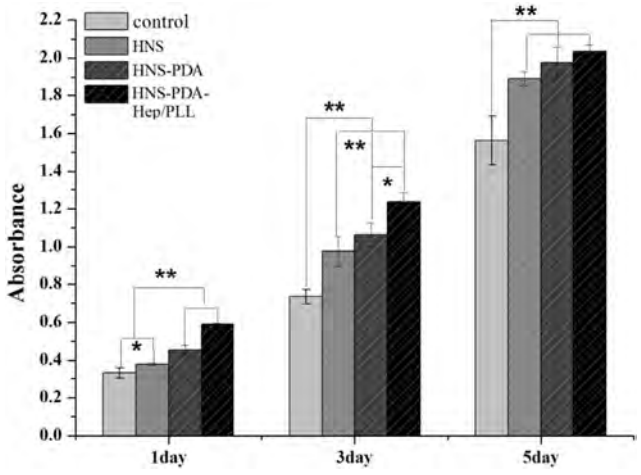

Fig. 9. Proliferation of HUVECs cultured on different samples measured by MTT. After cultivation for 1 day, HNS-PDA and HNS-PDA-Hep/PLL microspheres show a significant effect on HUVECs proliferation rates compared with the control group. After 3 days and 5 days, all the origin HNS, HNS-PDA and HNS-PDA-Hep/PLL microspheres showed significant promotion on HUVECs proliferation rates. *and ** indicate significant difference ($P < 0.05$) and highly significant difference ($P < 0.01$).

3.3.3. APTT, PT and TT

Activated partial thromboplastin time (APTT), prothrombin time (PT) and thrombin time (TT) were measured to further evaluate the anticoagulation potency of microsphere-immobilized samples. The APTT values of plasma after incubation with Hep/PLL microsphere-immobilized surfaces was significantly prolonged compared to HNS and HNS-PDA and there was almost no coagulation for HNS-PDA-Hep/PLL microsphere samples (Fig. 6A). The mean APTT value of HNS-PDA-Hep/PLL microspheres was prolonged by approximately 50 s in comparison with HNS and HNS-PDA. This indicated a significant improvement in the anticoagulant property. However, the effect of Hep/PLL microspheres on the PT value appeared quite weak compared to APTT with only 2 s prolongation (Fig. 6B). The TT value was extended to 36 s on HNS-PDA-Hep/PLL microsphere sample surfaces (Fig. 6C), prolonged by nearly 20 s in comparison with HNS and HNS-PDA. This indicated that Hep/PLL microsphere-immobilized surfaces exert a favorable effect on preventing fibrin-induced platelet adhesion.

3.3.4. Fibrinogen

Fig. 6D shows the surface fibrinogen(Fbg) content of each sample assay. We can conclude that the surface Fbg content of HNS and HNS-PDA was almost the same as that for PPP. HNS-PDA-Hep/PLL microsphere surface Fbg was significantly reduced, mainly due to the electrically negative Hep that inhibited the activity of thrombin fibrinogen, resulting in good blood compatibility.

3.4. Cellular compatibility evaluation in vitro

3.4.1. Cell morphology characterization analysis

The HUVEC cells on the surface of HNS, HNS-PDA and HNS-PDA-Hep/PLL microspheres almost formed a single layer. The cells kept their natural original shape, spindle or irregular triangular, extending freely, without significant difference among them (Fig. 7). Five SEM views at 800× magnification were selected randomly to make statistical analysis for the adhesion of cells (Fig. 8). Adhesion cell numbers were significantly different between HNS-PDA-Hep/PLL microspheres and HNS-PDA($P < 0.01$), and with no significant difference between HNS-PDA and HNS($P > 0.05$). This indicated that the HNS-PDA to cell adhesion effect was not significant. The results suggest that the HNS surface with Hep/PLL microsphere-immobilized was beneficial for cell proliferation, and hence possesses a better cell compatibility.

Table 3
Effect of samples surface on the NO, T-AOC content of the HUVECs supernatant.

Groups	NO(μmol/L)	T-AOC(unit/mL)
Control	70.23 ± 0.82	2.88 ± 0.13
HNS	91.60 ± 1.86[b]	3.41 ± 0.44[a]
HNS-PDA	90.00 ± 1.16[b]	3.21 ± 0.47[b]
HNS-PDA-Hep/PLL microsphere	101.05 ± 0.90[b]	4.69 ± 0.54[b]

[a] Significant difference ($P < 0.05$).
[b] Highly significant difference ($P < 0.01$).

3.4.2. Cytotoxicity test

The RGR of HUVEC cells was evaluated by MTT assay to evaluate cell proliferation. Detailed test results are shown in Fig. 9. After cultivation for 1 day, HNS-PDA and HNS-PDA-Hep/PLL microspheres show a significant effect on HUVECs proliferation rates compared with the control group. After 3 days and 5 days, all the origin HNS, HNS-PDA and HNS-PDA-Hep/PLL microspheres showed significant promotion on HUVECs proliferation rates. This indicated that HNS was stable and without poisonous substance precipitation or other obvious side effects on cells. Furthermore, the surface of HNS with Hep/PLL microspheres has a better promoting effect on cell proliferation.

3.4.3. NO release and T-AOC test

NO, the endothelium-derived relaxing factor, played a key role in the maintenance of vascular homeostasis by inhibiting excessive vascular SMC proliferation, platelet aggregation and leukocyte adhesion. Compared with the NO content in normal cells, HNS, HNS-PDA and HNS-PDA-Hep/PLL microspheres all had significantly increased NO content (Table 3). We can conclude theoretically that this will inhibit leukocyte and platelet adhesion to HUVECs to reduce the degree of cell damage. T-AOC results indicated that HNS-PDA-Hep/PLL microspheres significantly increased HUVECs total antioxidant capacity, which could mop up the reactive oxygen in vivo more efficiently to prevent oxidation-induced oxidative stress response.

4. Discussion

In this study, the surface of medical grade high nitrogen nickel-free austenitic stainless substrates were functionalized with Hep/PLL microspheres. We demonstrated that PDA-Hep/PLL microsphere-immobilized high nitrogen nickel-free austenitic stainless substrates stimulated the growth of HUVECs, inhibiting blood coagulation.

Roughness of the surface is very important for implanted material in contact with blood, because the surface roughness of the material will affect the plasma protein adsorption and platelet adhesion. Usually, for the vascular implant material and materials in contact with blood, if the roughness of the surface is <50 nm, there will be no effect on blood compatibility. However, if the roughness is >50 nm, it will promote plasma protein adsorption and platelet adhesion. This will result in formation of blood clots, influencing blood compatibility of the implant material. Surface functionalization of titanium substrates with Hep/PLL microspheres was achieved by initially introducing polydopamine as an intermediate layer for two reasons. Firstly, the surface of a native titanium substrate has only few active chemical groups to be used for efficient immobilization of Hep/PLL microspheres molecules. Secondly, dopamine-assisted surface modification of various materials was widely reported in recent years [34–35]. Dopamine is an analog of adhesive proteins in mussel with good biocompatibility. It was easily auto-polymerized to form polydopamine under weak alkaline condition [36].

Hep has been widely used as an anticoagulant and possesses incomparable advantages, such as suppression of intimal hyperplasia. Furthermore, it has anti-inflammatory properties and promotes endothelium regeneration in some cases. However, Hep does not react with dopamine due to lack of amine groups. Although several studies have

successfully conjugated Hep to dopamine via a chemical crosslinking approach [37–38], it appears difficult to maintain the bioactivity of Hep and to control the grafting density. PLL is commonly used to coat tissue cultureware to promote cell adhesion. As a cationic polyelectrolyte, PLL has frequently been used for gene loading and transfection [39–41]. In this study, positively charged PLL strongly interacted with the negatively charged Hep and formed microspheres in PBS via intermolecular electrostatic interaction. Although a similar concept has been reported by Park et al. [42], the microsphere preparation approach and the experimental system of the present study were significantly different. The presence of PLL introduced abundant amine groups to the microspheres, which contributed to covalent binding of the microspheres to the dopamine-coated surface via a Schiff base reaction and thereby facilitated surface heparinization.

An ideal combination of surface chemistry and biology is necessary for cardiovascular devices to satisfy clinical requirements. Hence, the bioactivity, quantity and durability of immobilized functional molecules are important. Nevertheless, they also pose major limitations. In this work, Hep was immobilized on dopamine-coated surface in the form of microspheres. The bioactivity of Hep was well retained and the durability of the material proved excellent. The optimum amount of Hep to selectively direct platelet and vascular cell behavior was also screened by biological evaluation of controlled Hep surface concentrations. However, this still appears insufficient to regulate HUVEC mobilization and migration, which is critical in re-endothelialization of cardiovascular devices. Future studies in our group will take advantage of the specific interaction of Hep with numerous growth factors and specific cytokine-loaded microspheres will be prepared to further resolve these shortcomings.

5. Conclusions and perspectives

In summary, Hep/PLL microspheres were immobilized onto the surface of medical grade high nitrogen nickel-free austenitic stainless steel substrates via polydopamine as an intermediate layer. Successful immobilization of Hep/PLL microspheres was confirmed by Zeta, AFM, HNSPS and contact angle measurements. The presence of Hep/PLL microspheres on the medical grade high nitrogen nickel-free austenitic stainless steel surfaces improved the cytocompatibility. In vitro cytocompatibility and blood compatibility tests demonstrated that HNS-PDA-Hep/PLL microsphere substrates exhibited excellent stability and anticoagulant activity. More importantly, we found that HNS-PDA-Hep/PLL microsphere substrates efficiently accelerated endothelialization and anticoagulation. Consequently, this work has potential application for the design of coronary artery stent surfaces tailored for vascular cell behavior.

Acknowledgements

This research program was supported by grants from the National Natural Science Foundation of China (11332003, 31370949, 31271014), the Key Project of National Science and Technology Support Program (No. 2012BAI18B02), the cooperative project of Chongqing Key Laboratory of Nano/Micro Composite Materials and Devices (CQKL-1502), and the Chongqing Graduate Student Research Innovation Project (CYS-14023) as well as Chongqing Science and Technology Commission (CSTC2013KJRC-LJRCCJ1000, CSTC2015JCYJBX0003). The authors also thank Mr Xingzheng Zou from Chongqing Institute of Materials for providing some experimental materials as well as the support of the Public Experiment Center of State Bio-industrial Base, Chongqing, China.

References

[1] K.K. Howard, J.J. Piotrowski, S. Kumanyika, J.E. Fielding, Health Educ. Behav. 38 (2011) 551–557.
[2] Q.L. Li, J.L. Chen, C. Chen, Z.Y. Chen, J.Y. Chen, N. Huang, J. Biomed. Mater. Res. A 95 (2010) 341–349.
[3] C.F. Luo, Y.M. Zheng, Z.J. Diao, J.H. Qiu, G.X. Wang, J. Med. Biol. Eng. 31 (2011) 307–316.
[4] X. Wu, G.X. Wang, C.J. Tang, D.C. Zhang, Z.G. Li, D.Y. Du, Z.C. Zhang, J. Biomed. Mater. Res. A 98 (2011) 442–449.
[5] S. Meng, Z.J. Liu, L. Shen, Z. Guo, W. Zhong, Q.G. Du, J.B. Ge, Biomaterials 30 (2009) 2276–2283.
[6] S. Elezi, A. Kastrati, F.J. Neumann, M. Hadamitzky, J. Dirschinger, Circulation 98 (1998) 1875–1880.
[7] I.T. Meredith, S. Verheye, C.L. Dubois, J. Dens, J. Fajadet, D. Carrie, S. Walsh, K.G. Oldroyd, O. Varenne, S.E. Jack, R. Moreno, A.A. Joshi, D.J. Allcocco, K.D. Dawkins, J. Am. Coll. Cardiol. 59 (2012) 1362–1370.
[8] Q. Liu, H.N.S.N. Cheng, H.H.N.S. Fei, J. Med. Biol. Eng. Comput. 49 (2011) 359–364.
[9] L.B. Pertile, P.M.S. Silva, V.B. Peccin, R. Peres, P.G. Silveira, C. Giacomelli, F.C. Giacomelli, M.C. Fredel, A. Spinelli, J. Biomed. Mater. Res. A 89A (2009) 1072–1078.
[10] T. Jiang, G.X. Wang, J.H. Qiu, L.L. Luo, G.Q. Zhang, J. Med. Biol. Eng. 29 (2009) 102–107.
[11] T.T. Zhao, Y. Li, Y.Z. Gao, Y. Xiang, H. Chen, T. Zhang, J. Mater. Sci. Mater. Med. 22 (2011) 2311–2318.
[12] M.H. Li, T.Y. Yin, Y.Z. Wang, F.F. Du, X.Z. Zou, H. Gregersen, G.X. Wang, Mater. Sci. Eng. C 43 (2014) 641–648.
[13] G. Li, P. Yang, W. Qin, M.F. Maitz, S. Zhou, N. Huang, Biomaterials 32 (2011) 4691–4703.
[14] I. Bjork, U. Lindahl, Mol. Cell. Biochem. 48 (1982) 161–182.
[15] R.A. Hoshi, R. Lith, M.C. Van, J.B. Jen, K.A. Allen, G. Lapidos, Ameer, Biomaterials 34 (2013) 30–41.
[16] Y.K. Ahn, M.H. Jeong, J.W. Kim, S.H. Kim, J.H. Cho, J.G. Cho, et al., Catheter. Cardiovasc. Interv. 48 (1999) 324–330.
[17] J.P. Boyle, R.H. Smart, J.K. Shirey, Am. J. Cardiol. 14 (1964) 25–28.
[18] HE. Conrad. New York, London: Academic Press. 1998.
[19] J. Yu, A.J. Wang, Z.Y. Tang, J. Henry, B.L.P. Lee, Y.Q. Zhu, et al., Biomaterials 33 (2012) 8062–8074.
[20] A.A. Khorana, A. Sahni, O.D. Altland, C.W. Francis, Arterioscler. Thromb. Vasc. Biol. 23 (2003) 2110–2115.
[21] Z.L. Yang, Q.F. Tu, J. Wang, N. Huang, Biomaterials 33 (2012) 6615–6625.
[22] H.G. Wang, T.Y. Yin, S.P. Ge, Q. Zhang, Q.L. Dong, D.X. Lei, D.M. Sun, G.X. Wang, Biomed. Mater. Res. A. 101 (2013) 413–420.
[23] S.E. Sakiyama-Elbert, Acta Biomater. 10 (2013) 1581–1587.
[24] S. Liu, T. Liu, J. Chen, M. Maitz, C. Chen, N. Huang, J. Biomed. Mater. Res. A 101 (2013) 1144–1157.
[25] H. Chen, Y. Chen, H. Sheardown, M.A. Brook, Biomaterials 26 (2005) 7418–7424.
[26] B. Joddar, A. Albayrak, J. Kang, M. Nishihara, H. Abe, Y. Ito, Acta Biomater. 9 (2013) 6753–6761.
[27] Z.L. Yang, Q.F. Tu, Y. Zhu, R.F. Luo, N. Huang, et al., Adv. Healthc Mater. 1 (2012) 548–559.
[28] J.S. Park, K. Park, D.G. Woo, H.N. Yang, H.M. Chung, K.H. Park, Small 4 (2008) 1950–1955.
[29] T. Merdan, J. Kopecek, T. Kissel, Adv. Drug Deliv. Rev. 54 (2002) 715–758.
[30] X. Gu, Y.F. Zheng, Y. Cheng, S.P. Zhong, T.F. Xi, Biomaterials 30 (2009) 484–498.
[31] Z.J. Li, X. Gu, S.Q. Lou, Y.F. Zheng, Biomaterials 29 (2008) 1329–1344.
[32] G.X. Wang, S.P. Ge, Y. Shen, H.G. Wang, Q.L. Dong, Q. Zhang, J.C. Gao, Y. Wang, Mater. Sci. Eng. C 32 (2012) 2190–2198.
[33] Z.L. Yang, Q.F. Tu, J. Wang, N. Huang, Biomaterials 33 (2012) 6615–6625.
[34] C.Y. Chien, T.Y. Liu, W.H. Kuo, M.J. Wang, W.B. Tsai, J. Biomed. Mater. Res. Part A 101A (2013) 740–747.
[35] N.G. Rim, S.J. Kim, Y.M. Shin, I. Jun, D.W. Lim, J.H. Park, H. Shin, Colloids Surf. B: Biointerfaces 91 (2012) 189–197.
[36] H. Lee, S.M. Dellatore, W.M. Miller, P.B. Science 318 (2007) 426–430.
[37] Y.K. Joung, S.S. You, K.M. Park, D.H. Go, K.D. Park, Colloids Surf. B: Biointerfaces 99 (2012) 102–107.
[38] Y.S. Jung, J.H. Jeong, S. Yook, B.H. Im, J. Seo, S.W. Hong, et al., Biomaterials 33 (2012) 295–303.
[39] J. Dai, S. Zou, Y. Pei, D. Cheng, H. Ai, H.N.S. Shuai, Biomaterials 32 (2011) 1694–1705.
[40] D. Zhou, C. Li, Y. Hu, H. Zhou, J. Chen, Z. Zhang, et al., Int. J. Biol. Macromol. 50 (2012) 965–973.
[41] M. Yamagata, T. Kawano, K. Shiba, T. Mori, Y. Katayama, T. Niidome, Bioorg. Med. Chem. 15 (2007) 526–532.
[42] K. JS Park, D.G. Park, H.N. Woo, H.M. Yang, K.H. Chung, Park, Small 4 (2008) 1950–1955.